Green-Function Calculations of Coherent Electron Transport in a Gated Si Nanowire

Young-Jo Ko, Mincheol Shin, Jeong Sook Ha, and Kyoung Wan Park

We describe a detailed numerical scheme to calculate electron transport in quantum wires using the Green function formalism combined with tight-binding orbital basis. As an example of the application, we study the electron transport in a Si nanowire containing a finite potential barrier. The effects of nonzero bias, temperature, and disorder on the barrier-induced oscillatory conductance are investigated within the context of coherent transport model. The oscillatory behavior of the conductance as a function of the Fermi energy is found to be highly sensitive to sample disorder and limited to a very low temperature and a small bias range.

Manuscript received May 17, 2000; revised August 1, 2000.

This work was supported by the MIC and the MOST-NRL project.

The authors are with the Telecommunication Basic Research Laboratory, ETRI, Taejon, Korea.

Young-Jo Ko (phone: +82 42 860 4810, e-mail: koyj@etri.re.kr)

Mincheol Shin (phone: +82 42 860 6036, e-mail: mcshin@etri.re.kr)

Jeong Sook Ha (phone: +82 42 860 5372, e-mail: jsha@idea.etri.re.kr)

Kyoung Wan Park (phone: +82 42 860 5608, e-mail: kwpark@idea.etri.re.kr)

I. INTRODUCTION

In the last decade, advances in nanofabrication technology have raised a lot of interest in electron transport in nanostructures such as quantum wires, dots, and molecules. In particular, with the development of Si based technology, it became possible to fabricate Si based wires as narrow as several nanometers wide [1]–[4]. In such a small system, the electronic behavior is governed by quantum mechanical principles, and its modeling frequently requires an accuracy of atomic level details. Recently, several authors have adopted Green function techniques [5] for the investigation of electron transport at an atomic level. By combining the fully quantum mechanical transport theory with traditional electronic structure tools based on atomic orbitals, it was possible to incorporate realistic band structures and atomistic structural details into quantum transport calculations. Examples of such calculations include the studies of electron transport in carbon nanotubes [6], metal nanowires [7], [8], atomic chains [9], and molecules [10], [11].

In this paper, we describe a detailed calculational procedure and provide an efficient numerical scheme for the Green function calculations of coherent transport in three-dimensional quantum wires. The Green function method is then used to study coherent electron transport through a square potential barrier in a Si[100] nanowire described by a semi-empirical tight binding (TB) model.

II. METHOD OF CALCULATIONS

The geometry of the wire system considered here is shown in Fig. 1, where the quantum wire is divided into three regions, namely, device region, semi-infinite left and right lead regions. In the semi-infinite leads, electrons are in thermal equilibrium

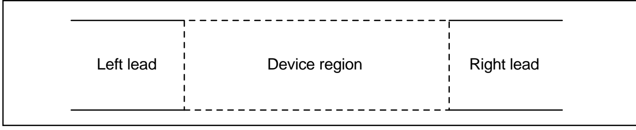

Fig. 1. Schematic view of a quantum wire connected to two semi-infinite wire contacts.

with chemical potentials μ_l and μ_r at the left and right leads, respectively. We consider phase-coherent transport of electrons through the device region from the left to right lead of the wire. The current for the coherent transport under a bias voltage $V = (\mu_l - \mu_r)/e$ is obtained by using the multi-channel Laudauer-Büttiker formula:

$$I(V) = \frac{2e}{h} \int T(E,V)[f_l(E) - f_r(E+V)]dE, \quad (1)$$

where $f_l(E)$ and $f_r(E)$ are the Fermi-Dirac distribution functions for the left and right lead electrons, respectively. Within the non-equilibrium Green function formalism [5], the transmission function $T(E,V)$ at a given bias voltage V is expressed in terms of the Green function for the device region G_d and the coupling function $\Gamma_{r,l}$ between the device and lead regions:

$$T(E,V) = Tr[\Gamma_l G_d \Gamma_r G_d^+], \quad (2)$$

where

$$G_d = [EI - H_d - \sum_l^R - \sum_r^R]^{-1} \quad (3)$$

$$\Gamma_{r,l} = i(\sum_{r,l}^R - \sum_{r,l}^A) \quad (4)$$

In the above equations, H_d is the Hamiltonian for the device region and the terms $\Sigma_{r,l}^R$ and $\Sigma_{r,l}^A$ are called retarded and advanced self energies, respectively, and are given by the relation $\Sigma_{r,l}^R = V_{r,l} G_{r,l}^R V_{r,l}^t$ and $\Sigma_{r,l}^A = V_{r,l} G_{r,l}^A V_{r,l}^t$, where $V_{r,l}$ is the coupling matrix between the right or left lead and the device region. $G_{r,l}^R (G_{r,l}^A)$ is retarded (advanced) Green function for the isolated semi-infinite right or left lead. The $G_{r,l}^{R,A}$ for wire structures is a symmetric matrix from the definition of the Green function $(E-H)G = I$, where the tight binding Hamiltonian H is real and symmetric. Since $[G_{r,l}^R]^+ = G_{r,l}^A$ and $G_{r,l}^{R,A}$ is symmetric, $\Sigma_{r,l}^A = \Sigma_{r,l}^{R*}$. Thus, $\Gamma_{r,l}$ can be rewritten as

$$\Gamma_{r,l} = -2\,\mathrm{Im} \sum_{r,l}^R = -2\,\mathrm{Im}\, V_{r,l} G_{r,l}^R V_{r,l}^t . \quad (5)$$

We employ atomic orbitals as a basis set in the construction of the wire Hamiltonians. If the total number of atoms within the device region is N_a and l_0 localized orbitals are used for each atom, the Green function G_d is a matrix of dimension $N_a \times l_0$, whereas the Green functions G_r^R and G_l^R for the semi-infinite leads are infinite dimensional. However, the use of localized orbitals confines the coupling between the device region and the lead to a finite region around the device-lead junction. Hence, $V_{r,l}$ has a finite number of nonzero elements and thus, only a finite number of matrix elements of G_r^R and G_l^R are necessary in obtaining $T(E,V)$. If the numbers of orbitals involved in the device-lead interaction are *m* and *n* in the lead and the device regions, respectively, the retarded self energy term $\Sigma_{r,l}^R = V_{r,l} G_{r,l}^R V_{r,l}^t$ and the coupling function $\Gamma_{r,l}$ contain *mm* non-zero elements. These non-zero elements can be arranged to form an $m \times m$ sub-matrix. We denote these non-zero sub-matrix part of $\Sigma_{r,l}$ as $\sigma_{r,l}$ and the necessary part of $\Gamma_{r,l}$ as $\gamma_{r,l}$, both of which are of the same matrix size $m \times m$. Also, we can see that only an $m \times m$ sub-matrix part of $G_{r,l}$ is involved in the self-energy terms because of the finite number of non-zero elements in $V_{r,l}$. This finite sub-matrix part of $G_{r,l}$ is denoted as $g_{r,l}$ and can be viewed as the surface Green function of the semi-infinite lead. We use a highly efficient iterative technique developed by López Sancho *et al.* for the calculation of surface Green functions, in which transfer matrices are obtained by incorporating 2^n layers at *n*-th iteration [12].

For short wires, the most time-consuming part lies in the calculation of the surface Green functions. However, for a wire with relatively longer device region, the calculation of G_d also becomes computationally demanding. Here, we describe an efficient numerical scheme to obtain G_d. We partition the device region into *n* layers so that each layer interacts only with its adjacent layers. If we denote the interaction matrix between *i* and *j* layers as $H_{i,j}$, $H_{i,j}$ is a nonzero matrix only when $i-1 \le j \le i+1$. From (3) G_d then satisfies the following matrix equation:

$$\begin{bmatrix} A_1 & B_1 & 0 & 0 & 0 & 0 \\ B_1^t & A_2 & \cdot & \cdot & 0 & 0 \\ 0 & 0 & \cdot & \cdot & B_{n-2} & 0 \\ 0 & 0 & 0 & B_{n-2}^t & A_{n-1} & B_{n-1} \\ 0 & 0 & 0 & 0 & B_{n-1}^t & A_n \end{bmatrix} \begin{bmatrix} G_{d,11} \\ G_{d,12} \\ \cdot \\ \cdot \\ G_{d,1n} \end{bmatrix} = \begin{bmatrix} I \\ 0 \\ 0 \\ \cdot \\ 0 \end{bmatrix}$$

where $A_1 = EI - H_{1,1} - \sigma_l$ and $A_n = EI - H_{n,n} - \sigma_r$. $A_i = EI - H_{i,i}$ for $i = 2,3,\cdots,n-2,n-1$. $B_i = -H_{i,i+1}$ and $B_i^t = -H_{i+1,i}$ since $H_{i,j} = H_{j,i}^t$. We note that $T(E) = \mathrm{Tr}[\Gamma_l G_d \Gamma_r G_d^+] = \mathrm{Tr}[\gamma_l G_{d,1n} \gamma_r G_{d,n1}^+]$ where $\gamma_{r,l} = -2\,\mathrm{Im}\,\sigma_l = -2\,\mathrm{Im}\, V_{r,l} g_{r,l}^R V_{r,l}^t$. In addition, from the general relation $G^R = G^{A+}$, $G_{d,n1}^+$ is just

the hermitian conjugate of $G_{d,1n}$. Thus, only the sub-matrix $G_{d,1n}$ is required to be solved in the above matrix equation.

To obtain $G_{d,1n}$, we basically follow the numerical algorithm for the inversion of tri-diagonal matrices [13]. The number operations in the algorithm are replaced by appropriate matrix operations. The resulting numerical scheme to obtain $G_{d,1n}$ is as follows. For $k = 2, 3, \cdots n$, the following procedure is repeated with $C = I$ initially:

$$\begin{aligned} &M \leftarrow B_{k-1}^{t} A_{k-1}^{-1}, \\ &C \leftarrow -MC, \\ &A_k \leftarrow A_k - MB_{k-1}. \end{aligned}$$

Finally, $G_{d,1n}$ is obtained as $G_{d,1n} = CA_{n-1}$. This numerical scheme introduced here is found to be highly efficient, in comparison with commonly available algorithms for banded matrix inversion. In particular, since we only need to calculate the last block matrix of G_d, the computational time is reduced by a factor of *1/n*. Most CPU time is then used in the calculation of the lead Green function. However, once it is calculated for a given electron energy, it can be stored for further use. It is also helpful to notice that the lead Green function matrix $G_{r,l}^{R}$ is symmetric regardless of the wire shape, which reduces the memory requirement by half.

III. ELECTRON TRANSPORT IN A SI NANOWIRE WITH A SQUARE BARRIER

In this section, we apply the preceding method to the coherent electron transmission in an idealized Si nanowire. For the accurate description of the conduction sub-bands of the wire within the tight-binding approximation, we employ an $sp^3d^5s^*$ model, which was recently parametrized by Jancu *et. al.* [14] and was found to describe quite well up to the two lowest conduction bands as well as the valance bands of bulk Si. This tight-binding model is also found to accurately give effective masses at the conduction band edge states of bulk Si, which is essential for wire sub-band description because the relative positions of the wire sub-bands sensitively depend on the effective masses. The tight binding Hamiltonian for the wire may be written as follows:

$$H = \sum_{i\alpha} \varepsilon_{i\alpha} c_{i\alpha}^{+} c_{i\alpha} + \sum_{i\alpha j\beta} t_{ij}^{\alpha\beta} c_{i\alpha}^{+} c_{j\beta}, \tag{6}$$

where *i, j* run over the atomic sites and α, β denote the atomic orbitals. The hopping parameter $t_{ij}^{\alpha\beta}$ is restricted to the nearest neighbors. The influence of external potentials and disorder in the wire can be simulated by varying the on-site and hopping energy parameters. In the transport calculations, the required Green functions, $G_{r,l}^{R}$ and $G_{d,1n}$ are calculated based on the above TB Hamiltonian.

The atomic structure of an ideal Si(100) wire considered here is shown in Fig. 2(a). The unit cell of the ideal [100] Si wire consists of four Si(100) atomic layers with the unit length equal to the Si lattice constant a_0, 5.431 Å. The Si dangling bonds at the four faces of the wire are passivated by hydrogen atoms so that any hydrogen-related surface states do not appear in the band gap region. The Si wire considered here is denoted by $n \times m$, where *n* and *m* represent the number of Si atomic layers along the [110] and [$1\bar{1}0$] directions, respectively. The unit cell of the ideal wire is taken to be the principal layer in the transport calculations so that the interaction between the principal layers occurs only between the nearest neighbor layers. Our calculation of the transmission function has been performed on Cray-c90. For example, for the 5×5 wire with a device region $20a_0$ long, it typically takes ~ 23 and ~ 14 CPU sec in obtaining the lead and device region Green functions, respectively, at one energy point. The required CPU time scales with the system size as $\sim N^3$, where *N* is the matrix size of the principal layer, while it increases linearly with the length of the device region.

The conduction subband structure of the ideal 5×5 wire is shown in Fig. 2(b). The wire subband has a direct band gap of 3.467 eV and, at the band bottom, it is composed of four closely located subbands within an energy range of 30 meV, which are derived from the four valley states, off the wire axis, at the conduction band bottom of bulk Si. The remaining two valley states give rise to the two indirect subbands starting at around 320 meV. In Fig. 2(c), the transmission function of the 5×5 wire is shown. The transmission function starts with a quantized conductance of $G_0 = 2e^2/h$ and then has a very narrow quantization plateau of 3 G_0 at 26-28 meV (not resolved in the figure) and two broad ones of 4 G_0 and 6 G_0.

As an illustrative example, we investigate the electron transmission through a square potential barrier in the 5×5 wire. The single barrier structure can be thought of as one of the simplest to induce a controlled oscillating conductance, which may be applicable to multi-functional electron devices [15]. We consider a square potential barrier embodied in the 5×5 wire, first assuming that an atomically uniform barrier can be introduced into a finite segment of the Si wire by the gate electrode. It may be very difficult to experimentally realize such an atomically abrupt and uniform potential barrier with the gate electrode. In fact, the assumed gate action is much like inserting a hetero-material to form a hetero-junction barrier which is more desirable for the abrupt barrier formation. We also investigate the effects of deviations from the abrupt and uniform barrier structure on the conductance. The 5×5 wire may correspond to the narrowest one conceivable, providing large splitting between the wire subbands, and thus, broad plateaus of the quantized conductance. To observe clear

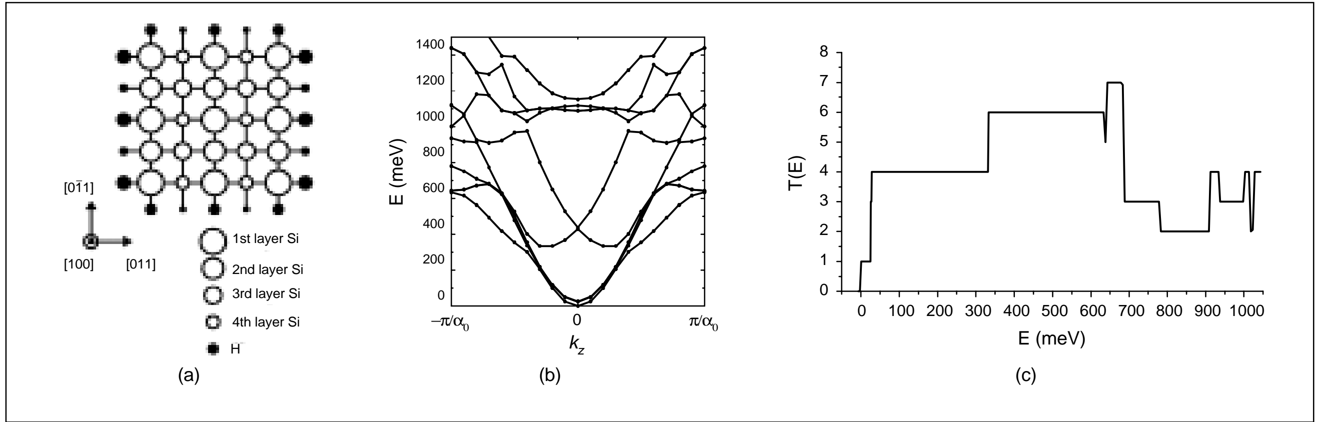

Fig. 2. (a) Cross-section of the atomic structure of the 5 × 5 Si[100] wire. The primitive cell of the wire consists of four atomic layers stacked along the [100] direction. (b) Subband structure of the 5 × 5 wire. (c) Transmission function *T(E)* of the 5 × 5 wire as a function of incoming electron energy *E*.

oscillatory peaks, a broad conductance plateau is desirable, otherwise, different resonance conditions between densely spaced subband states may result in a rather smooth conductance variation. However, as will be discussed later, these extremely narrow wires have inherent limitations in the operation because the presence of only a few defects can change the resonance condition randomly.

Once $T(E,V)$ is obtained, the current can be calculated using (1). Here, we use the following equivalent expression [16];

$$I(V) = \frac{1}{e}\int_{\mu_l}^{\mu_r=\mu_l-eV} G(E,V)dE, \qquad (7)$$

where the finite-temperature conductance function is defined as

$$G(E,V) = \frac{2e^2}{h}\int T(E',V)F_T(E'-E)dE', \qquad (8)$$

where $F_T(E)$ is the thermal broadening function given by

$$F_T(E) = -\frac{d}{dE}\left[\frac{1}{\exp^{(E/k_BT)}+1}\right] = \frac{1}{4k_BT}\operatorname{sech}^2\left(\frac{E}{2k_BT}\right) \qquad (9)$$

We first examine the variation of the conductance with changes of the barrier length and height. In Fig. 3, the transmission function is shown, as a function of incident electron energy relative to the conduction subband bottom, for three different barrier lengths of 5, 10, and $20a_0$ with various barrier heights. A common feature is oscillatory conductance superimposed upon ballistic conductance steps, thus, negative differential conductance, as a function of incident electron energy, which is caused by the interference between the incident electron waves and the waves reflected back and forth by the two end planes of the barrier [17]. With increasing the barrier length, more peaks of narrower and sharper shape are developed. The peak positions

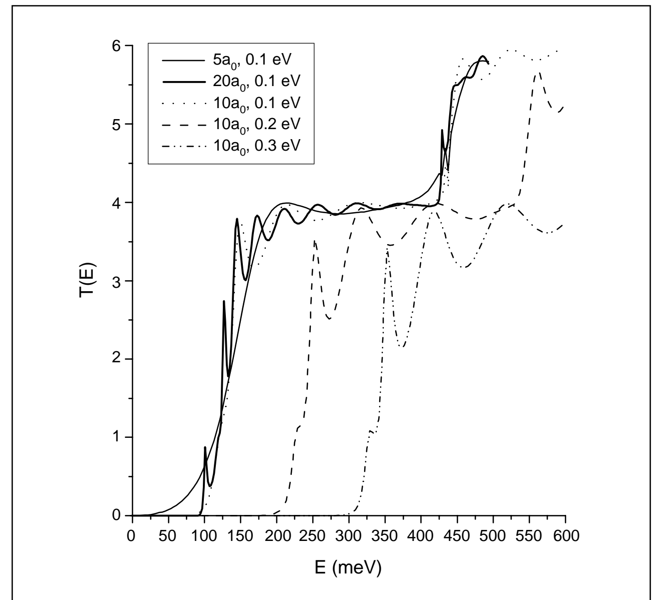

Fig. 3. Transmission function *T*(*E*) as a function of incoming electron energy *E* for the 5 × 5 wires with single square barrier potentials. Variations in *T*(*E*) between barriers with different lengths and different heights are compared. In the inset, the barrier length and height are indicated for each curve.

are approximately given by the resonance condition for a one-dimensional square barrier; $kL = n\pi$ with electron wave vector *k* and barrier length *L*. It is clearly seen that the average peak spacing reduces by half as the barrier length doubles from $10a_0$ to $20a_0$. In the case of the $5a_0$ long barrier, we observe a nonzero conductance at electron energies below the barrier height, which results from tunneling through the barrier. From the zero temperature conductances for the $10a_0$ long barriers with different barrier heights, it is found that a higher barrier induces stronger oscillations with more deepened dips. The overall features are in good agreement with electron transmission through a one-dimen-

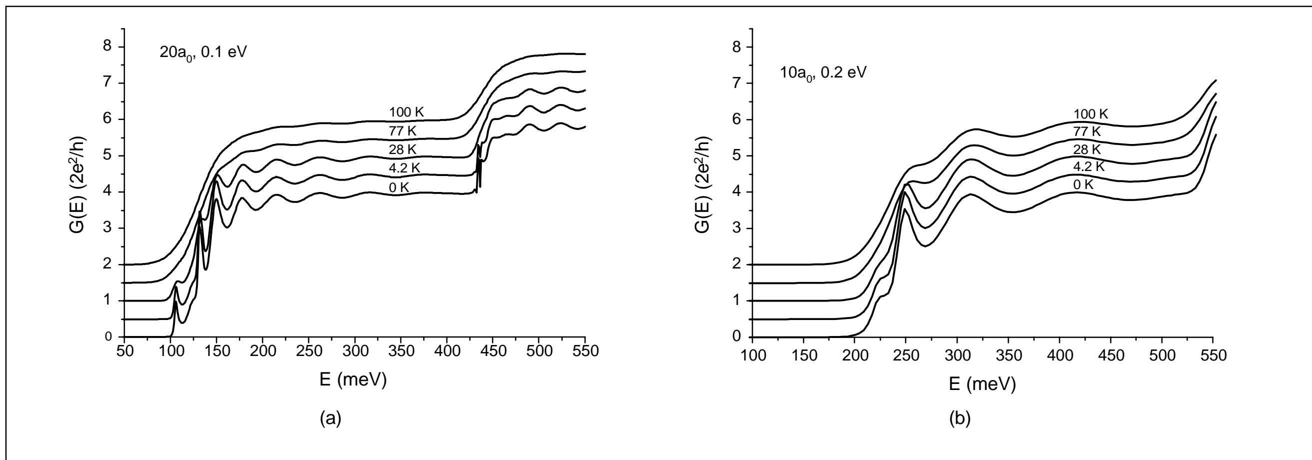

Fig. 4. Zero-bias conductance function $G(E)$ at various temperatures as a function of incoming electron energy E for the 5×5 wire with a square potential barrier. In (a), $G(E)$ is drawn for the barrier 0.1 eV high and $20a_0$ long and in (b) for the barrier 0.2 eV high and $10a_0$ long.

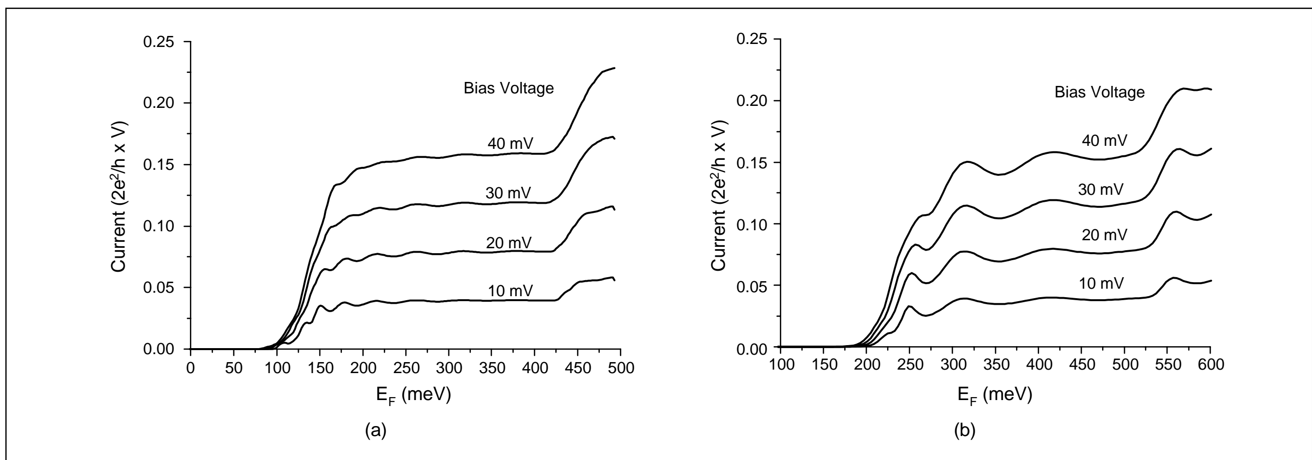

Fig. 5. Drain current $I(E_F)$ at zero temperature under small bias voltages V as a function of Fermi energy E_F for the 5×5 wire with a square potential barrier. In (a), $I(E_F)$ for the barrier 0.1 eV high and $20a_0$ long and in (b) for the barrier 0.2 eV high and $10a_0$ long.

sional square-potential barrier while different details are attributed to the multi-subband nature of the three-dimensional wire.

In (8), the finite-temperature conductance $G(E, V)$ is given by the convolution of the zero-temperature transmission function and the thermal broadening function, which has a width of $\sim k_B T$. At a nonzero temperature, detailed structures in the conductance within an energy range comparable to or smaller than the thermal broadening width are washed out. Because of the thermal broadening, narrow resonance peaks observed for long barriers at zero temperature are easily smoothed out as the temperature increases. However, too short barriers do not show significantly oscillatory conductance even at zero temperature. In Figs. 4(a) and 4(b), we show the temperature dependence of $G(E, V=0)$ for the $20a_0$ long barrier with 0.1 eV height and the $10a_0$ long barrier with 0.2 eV height, respectively. We observe that the sharp and narrow resonance peaks in the zero-temperature conductance of the $20a_0$ barrier in low electron energy region rapidly disappear with increasing temperature [Fig. 4(a)]. However, the rather smooth and broader oscillations caused by the lower energy $10a_0$ barrier are found to persist up to ~100 K [Fig. 4(b)].

To investigate the finite bias effect on the conductance, we calculate the current at different bias voltages assuming that the voltage drop occurs linearly across the device region which is here equal to the barrier region. In Fig. 5, the calculated drain current is shown as a function of the Fermi energy at zero temperature under small bias voltages. The small, finite bias voltage simply smoothes out the sharp resonance structures observed in the zero-temperature conductance, much like the finite temperature effects. By contrast, the application of a large bias shows additional features unique to a specific wire subband structure. Figure 6 shows calculated conductance functions in the cases with relatively large bias. Upon biasing, nonzero conductance appears at some electron energies below the barrier, as marked by A in the

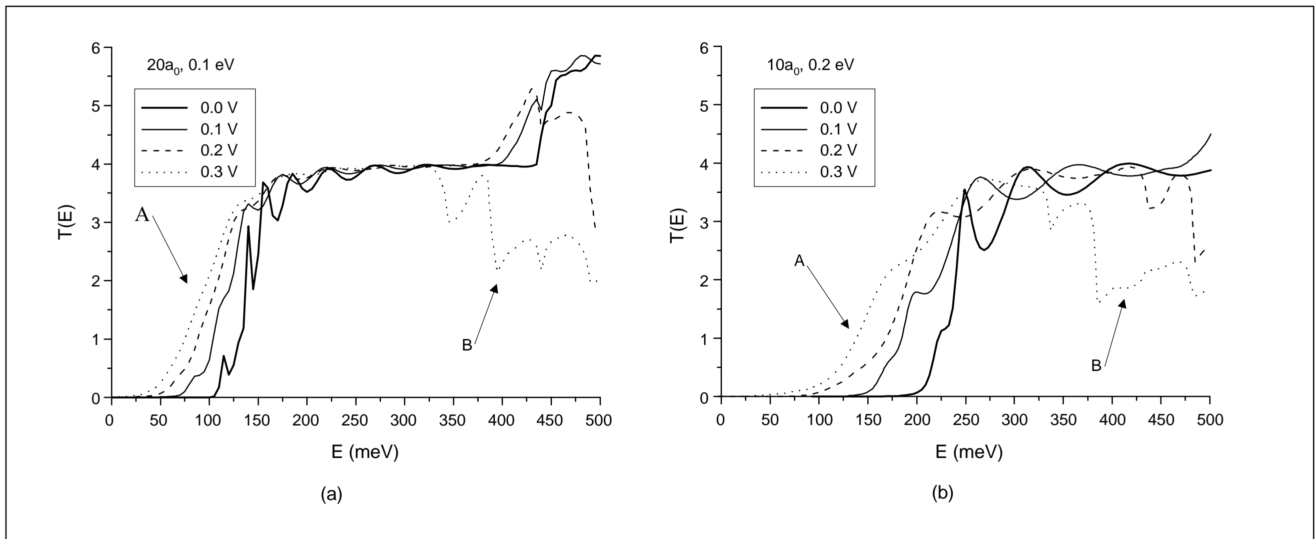

Fig. 6. Transmission function $T(E)$ for the 5×5 wire with a square potential barrier under large bias voltages. In (a), the barrier is 0.1 eV high and $20a_0$ long, and in (b), the barrier is 0.2 eV high and $10a_0$ long. In the insets, the bias voltage is indicated for each curve.

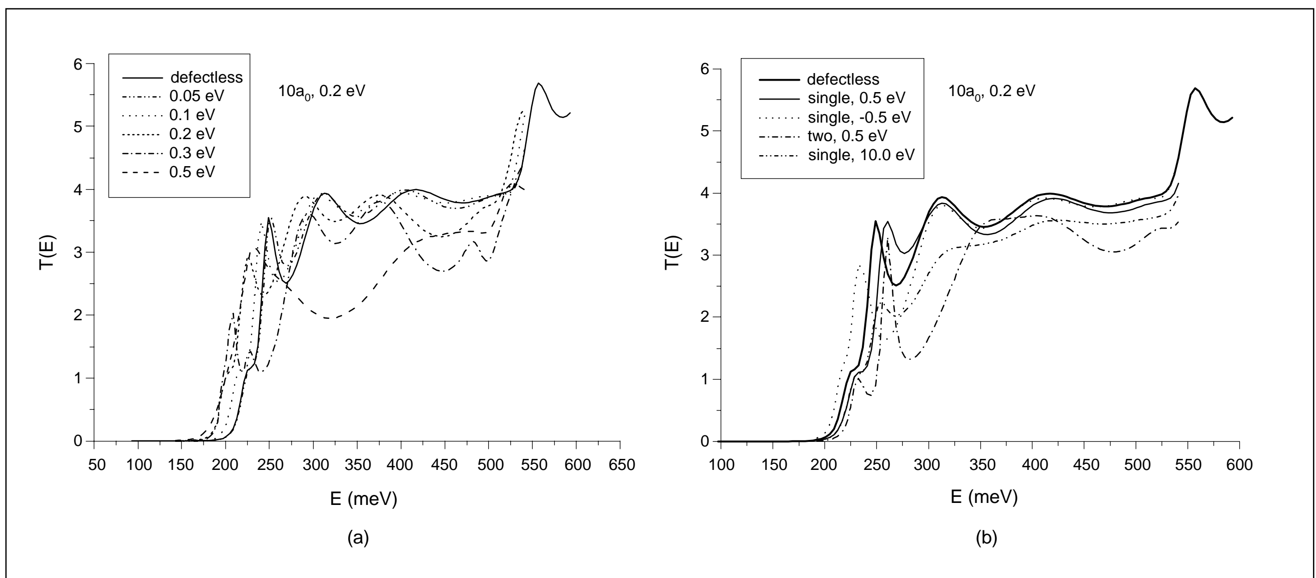

Fig. 7. Transmission function $T(E)$ for the 5×5 wire with a square potential barrier 0.2 eV high and $10a_0$ long (a) in the presence of uniform, on-site energy disorder with various disorder strengths and (b) in the presence of single or multiple defects within the barrier region

figure. At these energies, the finite bias reduces the effective barrier width, allowing the electrons to transmit via tunneling through the barrier. At energies higher than the barrier height, the transmission is also larger and smoother, in comparison with the unbiased case. This is because the resonance becomes weak as the reflection at the right end of the barrier is reduced with increasing bias.

Under large bias voltages, we observe decreasing conductance around a high-energy region marked by B in the figure. This decrease in the conductance originates from the subband structure of the wire; the number of available conducting channels at the drain (right lead) becomes smaller than that at the source (left lead) at this energy range. For example, at an electron energy of ~ 500 meV, the number of the conducting channels at the source is six, while the corresponding number is reduced to two at the drain under a bias voltage of 0.3 V [see Fig. 2(c)].

To study the effect of lattice disorder on the conductance, we introduce uniform disorder into the barrier region by adding a potential $\delta\varepsilon$ randomly chosen in the interval $-W \leq \delta\varepsilon \leq W$ to every lattice atom. We calculate conductance variation for the $10a_0$ long and 0.2 eV high barrier by changing the magnitude W of the uniform disorder. In Fig. 7(a), weak uniform disorder

with $W \leq 0.1$ eV along the barrier length does not induce a significant change in the conductance; the peak positions and shapes are little changed from those obtained without disorder. However, relatively strong disorder with $W \geq 0.3$ eV totally alters the overall conductance shape randomly from one disorder configuration to another.

The presence of isolated defects within the barrier region changes the phase-shift of electron waves acquired from traveling along the barrier, thereby changing the resonant energy positions. A defect is simulated by adding the same amount of $\delta\varepsilon$ to each on-site energy of the defected site. Generally, a positive (negative) defect potential induces effectively less (more) phase-shift along the barrier, shifting the resonance peak positions to the higher (lower) energy side. A single weak defect ($|\delta\varepsilon| \leq 0.1$ eV) is found to change the resonance positions by ≤ 10 meV and the peak values by $\leq 5\,\%$, regardless of the disordered sites (not shown), while a relatively strong defect ($|\delta\varepsilon| \sim 0.5$ eV) can induce a large change in the first peak, but with much diminished effect on the higher energy peaks as shown in Fig. 7(b). Although the existence of a few weak defects or a single strong defect in the wire little or partly change the conductance, the presence of a couple of strong defects can alter the conductance as a whole as, for example, two defects with $\delta\varepsilon = 0.5$ eV in Fig. 7(b). The above effects of the disorder and isolated defects hold true for other square barriers with different barrier heights, but a longer disordered region has more destructive effect on the conductance than a shorter one with the same strength of disorder.

IV. SUMMARY

In summary, we have developed an efficient numerical method to calculate coherent electron transport in quantum wires. The Green function formalism combined with tight-binding orbital basis enables efficient calculations of necessary Green functions. This method is applied to the electron transport in a Si nanowire with a square potential barrier. Resultant oscillatory conductance as a function of the Fermi energy is found to be quite vulnerable to the finite bias and temperature, limiting the observation of the conductance oscillations to a very low temperature and a small bias range. Under an applied bias voltage, the asymmetry in the barrier height brought by nonzero bias results in tunneling current and weaker reflection near the drain region, both of which suppress the resonance peaks. The current can be also suppressed by the application of a large bias exceeding a subband width which reduces the conduction channels at the drain. Finally, we have discussed the effects of random disorder and defects in the barrier region on the conductance.

REFERENCES

[1] H. I. Liu, D. K. Biegelsen, F. A. Ponce, N. M. Johnson, and R. F. W. Pease, "Self-limiting Oxidation for Fabricating Sub-5 nm Silicon Nanowires," *Appl. Phys. Lett.*, Vol. 64, No. 11, 1994, pp. 1383–1385.

[2] Y. Nakajima, Y. Takahashi, S. Horiguchi, K. Iwadate, H. Namatsu, K. Kurihara, and M. Tabe, "Fabrication of a Silicon Quantum Wire Surrounded by Silicon Dioxide and its Transport Properties," *Appl. Phys. Lett.*, Vol. 65, No. 22, 1994, pp. 2833–2835.

[3] H. Namatsu, K. Kurihara, M. Nagase, and T. Makino, "Fabrication of 2-nm-wide Silicon Quantum Wires through a Combination of a Partially-Shifted Resist Pattern and Orientation-Dependent Etching," *Appl. Phys. Lett.*, Vol. 70, No. 5, 1997, pp. 619–621.

[4] V. Ng and H. Ahmed, "Effect of Wire Length on Coulomb Blockade in Utrathin Wires of Recrystallized Hydrogenated Amorphous Silicon," *J. Appl. Phys.*, Vol. 86, No. 12, 1999, pp. 6931–6942.

[5] S. Datta, *Electronic Transport in Mesoscopic Systems*, Cambridge University Press, Cambridge, UK, 1995.

[6] M. P. Anantram and T. R. Govindan, "Conductance of Carbon Nanotubes with Disorder: a Numerical Study," *Phys. Rev. B*, Vol. 58, No. 8, 1998, pp. 4882–4887.

[7] J. C. Cuevas, A. L. Yeyati, and A. Martin-Rodero, "Microscopic Origin of Conducting Channels in Metallic Atom-Size Contacts," *Phys. Rev. Lett.*, Vol. 80, No. 5, 1998, pp. 1066–1069.

[8] M. Brandbyge, N. Kobayashi, and M. Tsukada, "Conduction Channels at Finite Bias in Single-Atom Gold Contacts," *Phys. Rev. B*, Vol. 60, No. 24, 1999, pp. 17064–17070.

[9] T. Yamada and Y. Yamamoto, "Energy Band for Manipulated Atomic Structures of Si, GaAs, and Mg on an Insulating Substrate," *Phys. Rev. B*, Vol. 54, No. 3, 1996, pp. 1902–1906.

[10] M. Magoga and C. Joachim, "Conductance and Transparence of Long Molecular Wires," *Phys. Rev. B*, Vol. 56, No. 8, 1997, pp. 4722–4729.

[11] Y. Xue, S. Datta, S. Hong, R. Reifenberger, J. I. Henderson, and C. P. Kubiak, "Negative Differential Resistance in the Scanning-Tunneling Spectroscopy of Organic Molecules," *Phys. Rev. B*, Vol. 59, No. 12, 1999, pp. R7852–R7855.

[12] M. P. López Sancho, J. M. López Sancho, and J. Rubio, "Quick Iterative Scheme for the Calculation of Transfer Matrices: Application to Mo(100)," *J. Phys., F: Met. Phys.*, Vol. 14, 1984, pp. 1205–1215.

[13] S. S.M. Wong, *Computational methods in physics and engineering*, World Scientific, Singapore, 1997.

[14] J.-M. Jancu, R. Scholz, F. Beltram, and F. Bassani, "Empirical $spds^*$ Tight-binding Calculation for CUBIC semiconductors: General Method and Material Parameters," *Phy. Rev. B*, Vol. 57, No. 11, 1998, pp. 6493–6507.

[15] M. Asada, "Electron-Wave Reection and Resonance Devices," *Mesoscopic Physics and Electronics*, edited by T. Ando, Y. Arakawa, K. Furuya, S. Komiyama, and H. Nakashima, Springer-Verlag, Berlin, Germany, 1998.

[16] P. F. Bagwell and T. P. Orlando, "Landauer's conductance formula and its generalization to finite voltages," *Phys. Rev. B*, Vol. 40, No.

3, 1989, pp. 1456–1464.
[17] A. Messiah, *Quantum mechanics* - Vol. I, North-Holland, Amsterdam, The Netherlands, Chap. 3, 1975.

Young-Jo Ko was born in Kwangju, Korea in 1970. He graduated from Kwangju high school of science in 1988 and received B.S., M.S., and Ph.D. degrees in physics from KAIST in 1992, 1994, and 1998, respectively. His research field, while at KAIST, was theoretical modeling of semiconductor surfaces and hetero-epitaxial growth from first-principles total-energy calculations. He joined the Telecommunication Basic Research Laboratory of ETRI in March 1998. His research interests include the atomic-scale modeling of semiconductor surfaces from first-principles, the atomic and electronic structure of nanostrucutures, and the transport properties of nanoelectronic devices. He is currently working on the numerical simulation of quantum transport in nanoelectronic devices.

Mincheol Shin was born in Hong Sung, Korea in 1965. He received the B.S. degree in physics from Seoul National University, Seoul, Korea in 1988 and the Ph.D. degree in physics from Northwestern University, Evanston, Illinois, USA in 1992. Since 1993, he has been with Research Department in ETRI working on theoretical modelings and calculations for mesoscopic systems.

Jeong Sook Ha graduated from Seoul National University with a B.S. degree in chemistry in 1984, and subsequently received a Ph.D. degree in chemistry from Brown University, USA in 1989. From 1989 to 1991, she worked as a postdoctoral fellow at the University of Chicago, USA. She joined the Research Department of ETRI in 1991. Her research interests include the fabrication and characterization of silicon nano-structures, surface chemical reactions in an atomic scale, and structure and electronic properties of semiconductor surfaces. She is a member of the Korean Chemical Society, Korean Vacuum Society, American Physical Society, and American Vacuum Society.

Kyoung Wan Park was born in Seoul, Korea in 1956. He received B.S. and M.S. degrees in physics from Seoul National University, Seoul, Korea in 1978 and from Korea Advanced Institute of Science, Seoul, Korea in 1981, respectively, and his Ph.D. degree in physics from North Carolina State University, Raleigh, North Carolina, USA in 1990. From 1981 to 1984, he was a researcher with the Optics Laboratory of Korea Standards Research Institute. In 1990, he joined Research Department in ETRI. His research interests include thin film growth of semiconductors, surface treatments and optical measurements on compound semiconductors, and mesoscopic phenomena.